Biogeosciences Discuss., 11, 4695–4727, 2014
www.biogeosciences-discuss.net/11/4695/2014/
doi:10.5194/bgd-11-4695-2014

Biogeosciences Discussions
Open Access

Low-level jets and above canopy drainage as causes for turbulent exchange in the nocturnal boundary layer

T.-S. El-Madany[1], H. F. Duarte[2], D. J. Durden[2,*], B. Paas[1,], M. J. Deventer[1], J.-Y. Juang[3], M. Y. Leclerc[2], and O. Klemm[1]**

[1]University of Münster, Climatology Working Group, Institute of Landscape Ecology, Münster, Germany
[2]The University of Georgia, Laboratory for Environmental Physics, Griffin, USA
[3]National Taiwan University, Department of Geography, Taipei, Taiwan
[*]now at: NEON Inc., Boulder, USA
[**]now at: University of Tübingen, Environmental Physics Department, Tübingen, Germany

Received: 24 January 2014 – Accepted: 17 March 2014 – Published: 25 March 2014

Correspondence to: T.-S. El-Madany (tarek.elmadany@uni-muenster.de)

Published by Copernicus Publications on behalf of the European Geosciences Union.

Abstract

SODAR (SOund Detection And Ranging), eddy-covariance, and tower profile measurements of wind speed and carbon dioxide were performed during 17 consecutive nights in complex terrain in northern Taiwan. The scope of the study was to identify the causes for intermittent turbulence events and to analyse their importance in nocturnal atmosphere–biosphere exchange as quantified with eddy-covariance measurements. If intermittency occurs frequently at a measurement site this process needs to be quantified in order to achieve reliable values for ecosystem characteristics such as net ecosystem exchange or net primary production.

Fourteen events of intermittent turbulence were identified and classified into above canopy drainage flows (ACDF) and low-level jets (LLJ) according to the height of the wind speed maximum. Intermittent turbulence periods lasted between 30 min and 110 min. Towards the end of LLJ or ACDF events, positive vertical wind velocities and, in some cases upslope flows occurred, counteracting the general flow regime at night time. The observations suggest that the LLJ and ACDF penetrate deep into the cold air pool in the valley, where they experience strong buoyancy due to density differences, resulting in either upslope flows or upward vertical winds.

Turbulence was found to be stronger and better developed during LLJs and ACDFs, with eddy-covariance data presenting higher quality. This was particularly indicated by spectral analysis and stationary tests.

Significantly higher fluxes of sensible heat, latent heat and shear stress occurred during these periods. During LLJ and ACDF, fluxes of sensible heat, latent heat, and CO_2 were mostly one-directional. For example, exclusively negative sensible heat fluxes occurred while intermittent turbulence was present. Latent heat fluxes were mostly positive during LLJ and ACDF with a median value of $34\,W\,m^{-2}$, while outside these periods the median was $2\,W\,m^{-2}$. In conclusion, intermittent turbulence periods exhibit a strong impact on nocturnal energy and mass fluxes.

BGD
11, 4695–4727, 2014

1 Introduction

During the last years, many investigations to study atmospheric processes that impact turbulence, and transport in the nocturnal boundary layer have been performed. Advection (Lee, 2004; Aubinet et al., 2005; Kutsch et al., 2008), drainage flows (Belcher et al., 2008; Mahrt, 2010), gravity waves (Zilitinkevich et al., 2009; Vecenaj et al., 2011; Zeri and Sa, 2011; Durden et al., 2013) and low-level jets (LLJ) (Banta et al., 2002; Mathieu et al., 2005; Darby et al., 2006; Karipot et al., 2008; Sun et al., 2012; Huang and Bou-Zeid, 2013) are the most commonly identified processes in this context. Advection, drainage flows, and LLJ can occur on slight slopes in rather homogeneous terrain (Mahrt, 1999; Aubinet, 2008), while gravity waves are usually caused by topographic changes or irregularities of the canopy top (Lee et al., 1997). In complex terrain, all of these processes may occur and large effort was made within projects like T-REX (Grubisic et al., 2008) and VTMX 2000 (Doran et al., 2002) to understand the physics behind such (nocturnal) flows and how they influence transport of matter and energy (Cooper et al., 2006; Pinto et al., 2006; Reinecke and Durran, 2009; Choukulkar et al., 2012).

In cases of a stably stratified nocturnal boundary layer, turbulence is usually initialized by processes producing shear e.g. drainage flows and gravity waves (Nakamura and Mahrt, 2005). This type of turbulence is referred to as intermittent turbulence or, as defined by Mahrt (1999), as global intermittency. It plays a major role in estimating nocturnal exchange of, e.g., CO_2, but there is no consensus on how to treat longer time series when intermittent turbulence occurs at times. Variable data window sizes can lead to an increase of estimated turbulent energy and mass fluxes of 10 to 15 % (Acevedo et al., 2006). Mauder et al. (2013) address the difficulty to identify intermittency within eddy-covariance data sets.

In this study, an instrumental set-up was deployed to identify types of flow patterns that cause intermittent turbulence in very complex terrain. Preliminary studies at Chi-Lan Mountain (CLM), a site in Northern Taiwan, showed that periods of strong

BGD
11, 4695–4727, 2014

intermittent turbulence may occur during the night. However, several questions could not be answered by using eddy-covariance data alone: (1) why is intermittency occurring under various nocturnal situations? (2) Is the intermittency caused by drainage flows? (3) Are gusts or larger wind systems responsible for the intermittency?

To answer these questions, the presented work combines ground based remote sensing with SODAR, near-surface turbulent flux measurements with the eddy-covariance method, and tower-based profile measurements of the CO_2-concentration. Additionally, the influence of intermittent turbulence on turbulent nocturnal exchange above the forest will be estimated.

2 Measurements and data analysis

2.1 Site description

Eddy-covariance, SODAR (SOund Detection And Ranging), and CO_2-profile measurements were performed at the *Chi-Lan* Mountain research site (CLM) in north-eastern Taiwan (24°35′ N, 121°24′ E). It is located in the upper part of a valley at an elevation of 1650 m a.s.l. (Fig. 1) (Chang et al., 2002). The valley is orientated from north-west (top) to south-east (bottom) with an average slope of 14°. The vegetation is dominated by a 50 year old plantation of *Chamaecypraris obtuse var. formosa* and *Chamaecyparis formosensis* trees with an average canopy height between 11 and 14 m above ground (m a.g.). The wind system at CLM is dominated by thermally driven daytime valley winds (from south-east) and night time mountain winds (from north-west) (Klemm et al., 2006; El-Madany et al., 2013).

2.2 Instruments and set-up

Two experimental towers were used in this study. One tower (T1) was equipped with two eddy-covariance systems and a profile system for CO_2, the second tower (T2) was

BGD
11, 4695–4727, 2014

used to operate the SODAR. Tower T2 is located at a distance of 20 m from T1 in SSE direction.

The two eddy-covariance systems, each consisting of a R3-50 sonic anemometer (Gill Instruments, Ltd., Lymington, Hampshire, UK) for measuring the three dimensional wind components as well as the sonic temperature and a LI-7500 (LI-COR Biosciences, Lincoln, Nebraska, USA) for measuring molar densities of CO_2 and H_2O were located at 5 m and 10 m above the average canopy height (which corresponds to 19 m and 24 m a.g.), respectively. Data were recorded and stored at 10 Hz sampling frequency.

Vertical profiles of CO_2 were measured with a LI-840 gas analyzer (LI-COR Biosciences, Lincoln, Nebraska, USA) consecutively at 8 levels on T1 (0.5, 1.0, 2.0, 4.0, 8.0, 13.2, 16.0, 24.0 m a.g.). The tubing for all levels had the same length (15 m). The sample flow rate was set to 0.5 L min^{-1} and an automatic system controlled the switching of the valves. Each level was sampled at the frequency of 1 Hz for 15 s and the mean of the readings from the last 3 s for each level was collected. Subsequently, all measured values within a 30 min period were averaged to 30 min profiles.

A monostatic phased array doppler SODAR (model SFAS; Scintec AG, Rottenburg, Germany) was set-up on T2 at 5 m above canopy height (m a.c.) including a large enclosure (Scintec AG) to reduce negative influence of ground clutter to the measurements. After extensive testing, the following hardware and software configuration settings were used. The SFAS was orientated perpendicular to gravity with a north offset of 100°. A multi-frequency mode was used to emit eight frequencies ranging from 3.059 to 4.843 kHz. Vertical profiles of the 3-D wind field between 10 and 305 m above the SFAS (25 to 320 m a.g.) with a vertical resolution of 5 m and a temporal resolution of 10 min were calculated.

With this combination of local (eddy covariance and CO_2-profiles) and remote sensing (SODAR) techniques, the vertical structure of the wind and temporal evolution of turbulent fluxes can be investigated.

BGD
11, 4695–4727, 2014

2.3 Data processing

Flux calculations for sensible heat, latent heat, momentum, and CO_2 were performed with Eddy Pro 4.1 (LI-COR Biosciences, Lincoln, Nebraska, USA) for each 30 min averaging period. Coordinate rotation was done with the planar fit method (Wilczak et al., 2001), linear detrending was used for trend removal, time lags were detected with covariance maximization, WPL correction (Webb et al., 1980) was performed to compensate density fluctuation in the open path gas analyzer, spectral corrections for high and low frequency loss were done according to Moncrieff et al. (1997) and Moncrieff et al. (in Lee et al., 2004), respectively. Quality checks were performed according to the *Spoleto agreement*, 2004 for CarboEurope-IP (Mauder and Foken, 2011). The quality is determined by the stationarity of the time series and by the difference between the modeled integral turbulence characteristics and the measured ones (Foken and Wichura, 1996). Data sets that are not stationary and show large differences between the modeled and the measured integral turbulence characteristics are of quality class 2 and were not further used in this study.

A short time Fourier-transform was used to derive spectral characteristics of turbulence (i.e. vertical wind velocity) during jet periods. A Hemming window of 300 s length with 50 % overlap and a frequency band between 5 and 0.004 Hz was used. This is short enough to achieve a good temporal resolution and long enough to capture small and medium size turbulence elements that contribute to the power spectral density (PSD).

The SODAR data was processed with the APRun 1.43 software (Scintec AG). Raw data was averaged for 10 min intervals and corrections such as ground clutter detection and removal were applied. For all cases in which data passed internal quality control (for further information see APRun Software Manual 2011), main data such as horizontal wind speed, wind components (u, v, w), wind direction, standard deviations of wind components (σ_u, σ_v, σ_w,), and backscatter are available. Additional interpolation of missing data within the profiles was unnecessary due to the consistency of the data

BGD
11, 4695–4727, 2014

sets. Data gaps only occurred at the upper end of the measurement range and were left as they were.

2.4 Data selection

From 27 June to 14 July 2010, 17 nights (20:00–05:30 LT) were available for data analysis. Nighttime data was visually inspected to identify periods with low-level jet (LLJ) activity and above canopy drainage flows (ACDF). From here on, the phrase "jet period" will be used for periods when either, LLJ or ACDF occurred, while "no-jet period" will be used for the nocturnal data excluding jet periods.

LLJ events are defined as periods with a local maximum of wind speed up to 270 m a.g. This limit was set because the upper end of the LLJ (decline of wind velocity) could not be clearly identified due to the upper limit of the SODAR measurements (320 m a.g.). Additionally, these putative LLJ showed no influence on the wind field close to the canopy. They were therefore discarded from further analysis.

ACDF are katabatic winds that are defined as periods in which the maximum horizontal wind speed occurs at the closest measurement level above the canopy (i.e. 5 m a.c.).

To be included into further analysis jet periods needed to last for at least 30 min so that they cover a full averaging period for the calculated fluxes.

Altogether, 14 events match the above mentioned criteria during the measurement period. They are listed in chronological order with duration, height above ground of the wind speed maximum, maximum wind speed, and its classification as LLJ or ACDF in Table 1.

Only eddy-covariance and CO_2-profile data that fell completely within a jet period are considered as affected by the jet period. If only a part of the flux averaging period falls within the jet period (e.g., 10 min or 20 min), data are considered as not affected. As mentioned above, only turbulent fluxes with quality classes 0 and 1 (Mauder and Foken, 2011) were used for the analysis of jet and no-jet periods.

BGD
11, 4695–4727, 2014

3 Results

3.1 Atmospheric conditions

During the measurement period, 8 low-level jets and 6 above canopy drainage flows were identified. The durations of the events were between 30 min and 110 min with a median of 60 min.

Before low-level jets or above canopy drainage flows occurred, the horizontal wind speeds were usually below 0.5 m s^{-1} throughout the vertical profile. The Monin–Obukhov stability parameter ζ, as calculated from sonic anemometer data, shows that typically weakly to moderately stable boundary layer conditions prevailed throughout the entire nights. At 5 m a.c., ζ was very similar for jet and no-jet periods, while at 10 m a.c., clearly higher values of ζ occurred during jet periods (Table 2). Here, nearly all situations were moderately stable while more than 25 % of the no-jet periods were weakly stable.

For both sonic anemometer measurement heights, the horizontal wind speed and turbulent kinetic energy (TKE) were higher for jet periods than for no-jet periods. A lower TKE at 10 m a.c. as compared to 5 m a.c. indicates that nocturnal turbulence is mainly produced by the roughness of the canopy. This is true for both jet periods and no-jet periods. During no-jet periods, the horizontal wind speed was higher at 10 m a.c. as compared to 5 m a.c. while for jet periods, no clear gradient was apparent. The missing gradient is a result of analyzing LLJ and ACDF together. For LLJ and ADCF higher wind speeds are at 10 m a.c. and 5 m a.c., respectively.

3.2 Low-level jets

Figure 2 represents a typical LLJ of 80 min duration. Twenty minutes before the LLJ started, the lower part of the nocturnal boundary layer (up to 250 m) is calm with wind speeds below 1 m s^{-1}. During the LLJ maximum, horizontal wind speeds of about 7 m s^{-1} occurred at altitudes between 60 m and 100 m above the SODAR. The

BGD
11, 4695–4727, 2014

respective wind direction was WNW and the vertical winds were clearly negative with speeds between −0.5 and −1.75 m s^{-1}. The end of the LLJ is characterized by a sudden reduction in horizontal wind speed. The horizontal wind speed drops to maxima of about 0.5–1.0 m s^{-1} throughout the profile and the vertical wind speed becomes very small with values around zero up to 100 m above the SODAR.

The termination of some jet periods is characterized by a change in wind direction of 180° (from WNW to ESE) and a reversal of the vertical wind component (Fig. 3). This corresponds to an upward flow of the wind within the valley. This upward flow is not always as clearly pronounced as in this case (Fig. 3). In some cases the change of horizontal wind direction does not occur, but a reversal of the vertical wind component is apparent. After the upward flow, which typically lasts for 10 to 20 min, the jet period is over and wind speeds are small throughout the vertical profile.

3.3 Above canopy drainage flows

A typical above canopy drainage flow, as shown in Fig. 4, is characterized by a very pronounced maximum of wind speed just above the canopy. In this case (Fig. 4), the 30 min mean wind speed as measured by the sonic anemometer at 24 m a.g. is 3.0 and 3.6 m s^{-1} at 19 m a.g., respectively. These measurements match well with the wind profile data measured by the SODAR which show a constant increase in the horizontal wind speed between 120 and 35 m a.g. The end of the drainage flow is characterized by a change in vertical wind speed from negative to positive, even though the wind direction is still from north-west.

3.4 CO_2 profiles

Carbon dioxide typically accumulates at the forest's surface during night time as a result of nocturnal respiration of soil and vegetation. Within the trunk space, the CO_2 mixing ratio decreases from the surface to the bottom of the canopy. Within the canopy itself,

BGD
11, 4695–4727, 2014

the CO_2 mixing ratios are more or less constant while above the canopy, a further decrease with increasing altitude is apparent in all cases (Fig. 5).

During the LLJ of 8–9 July (Fig. 2; 23:30 to 01:30 LT), the CO_2 gradient between 0.5 m and 24 m is reduced from 1.26 ppm m^{-1} to 0.78 ppm m^{-1}. The gradient between 24 and 8 m a.g. is only 0.09 ppm m^{-1}, indicating that the LLJ-induced turbulence intrudes into the canopy and leads to strong mixing of the air above and inside the canopy. This mixing even affects the trunk space, and the near-surface mixing ratio drops by 10 ppm. After termination of the LLJ, the gradient starts to build up again. Sixty to ninety minutes later, the profile shape and the magnitude of the gradient are back to "normal", i.e. the conditions before onset of the LLJ.

3.5 Turbulent exchange

3.5.1 Data quality

It was mentioned in Sect. 2.3 that data of quality class 2 are considered of minor quality in eddy-covariance. The fraction of 30 min periods with this quality class varies strongly for the various fluxes. For example, for no-jet periods, the sensible heat and CO_2 fluxes exhibited by 5 and 20 % higher fractions of quality class 2 data than for jet periods, respectively. In other words, jet period data were of better quality. The latent heat flux (LE) and shear stress (τ) are nearly of the same quality for no-jet and jet periods. Overall, latent heat flux data exhibit the least quality for no-jet and jet periods with 36 % of the data being quality class 2.

The percentile deviations from the steady state condition for the time series of wu, wT, and wCO_2 are significantly smaller for jet periods than for no-jet periods (Fig. 6). Far more data are below the 30 % threshold. According to Foken (2008) and Mauder and Foken (2011), if deviations are below 30 % for the steady state and ITC tests, the respective data sets fall into the best quality class. Consequently, this test also indicates a better quality for jet periods as compared to no-jet periods.

BGD
11, 4695–4727, 2014

For no-jet periods the ITC_w deviations are significantly smaller than for jet periods. Nevertheless, more than 50 % of the ITC_w values are smaller than the 30 % threshold for jet periods. For ITC_u, all quartile values are smaller under jet periods but the difference is not significant (Fig. 6). All quartile values of u^* are smaller for no-jet period as compared to jet periods. It can be stated that more turbulence is present during jet periods. For reliable eddy-covariance measurements at night, a minimum of turbulence is required. As described by Goulden et al. (1996), the friction velocity (u^*) should be larger than 0.17 $m\,s^{-1}$. For both jet and no-jet periods, 75 % of the data exceed this threshold. The u^* values during jet periods are clearly higher and therefore eddy covariance data tend to be of better quality.

3.5.2 Spectral characteristics

The spectral analysis performed reveals that small to medium size turbulence elements (1–0.005 Hz) strongly contribute to PSD during jet periods (Fig. 7, 23:30–00:30 LT). Spectral characteristics during this period are very similar to daytime spectral characteristics with fully developed turbulence (Fig. 7, 10:00–14:00 LT and 23:30–00:30 LT). On the other hand, for no-jet periods, small to medium size turbulence elements play only a minor role in contributing to the PSD. Furthermore, discontinuities in the time and frequency domain of the spectrogram (Fig. 7, 20:00–23:30 LT) indicate the presence of not well-developed turbulence. These patterns can be observed for all cases of jet periods no matter if it is a LLJ or an ACDF.

3.5.3 Fluxes

Flux data as presented here are of quality class 1 and 0, exclusively. Fluxes of sensible heat, latent heat, and shear stress are of significantly larger magnitude during jet periods as compared to no-jet periods (Fig. 8). During no-jet periods, the median of latent heat fluxes is close to zero and the 1st and 3rd quartiles are at −18 and +21 $W\,m^{-2}$, respectively. For jet periods, latent heat fluxes are clearly positive with 1st

BGD
11, 4695–4727, 2014

and 3rd quartiles of 9 and 58 $W m^{-2}$. The direction of the fluxes is positive and therefore directed from the vegetation into the atmosphere. During no-jet periods, sensible heat fluxes are mostly negative while for jet periods, they are only negative and of larger magnitude (Fig. 8). No significant difference occurred between CO_2 fluxes during no-jet periods and jet periods, respectively. Nevertheless, more positive fluxes occurred during jet periods and all quartile values were higher or less negative.

Exemplarily, Fig. 9 shows the fluxes before, during, and after the LLJ of 8 July 23:30–9 July 00:30 (Fig. 2). Strong negative sensible heat fluxes between $-60 W m^{-2}$ and $-90 W m^{-2}$ were present during the LLJ. At the same time, positive CO_2 fluxes transport carbon dioxide out of the forest into the atmosphere. Clearly positive latent heat fluxes occurred only during the last 30 min of the LLJ (00:00–00:30 LT). Friction velocity is largest during LLJ activity as mechanical turbulence is produced by friction between the moving air and the canopy.

4 Discussion

4.1 Origin of low-level jets and above canopy drainage flows

No information about the development of LLJ and ACDF or their driving processes can be deduced from the employed experimental setup. Nevertheless, it is clear that the initiation of the LLJ and ACDF must be upslope of the instrumental set-up because the wind direction was north-west for all observed jet periods.

The data clearly show that jet periods occurred under moderately stable to very stable boundary layer conditions with low horizontal wind speeds throughout the vertical profile (Figs. 2–4 and Table 2). Such situations favor the formation of katabatic winds (i.e. ACDF), especially when the synoptic forcing is small (Zangl, 2009). When decoupling between the surface layer and air aloft occurs, the development of a LLJ is likely (Stull, 1988). According to Mahrt (1999), cooling over sloped terrain leads to a time-dependent and height-dependent horizontal pressure-gradient force that sets

BGD
11, 4695–4727, 2014

conditions favorable for the development of the LLJ. Remarkably, all observed LLJ and ACDF follow the orientation of the valley and flow downward from north-west to south-east (Figs. 2–4). This is typical for a katabatic wind that occurs at the surface and has to follow the terrain in a valley. For LLJ this implies, that the decoupling between the surface layer and the air above where the LLJ forms e.g. at the top of an inversion, follows the valley slope.

Jet periods show continuous and well developed turbulence throughout wide frequency scales from their sudden beginning until their likewise sudden ending (Fig. 7, 23:30–00:30 LT). Assuming that the initiation of the jet period is between the mountain ridge and the location of the tower, and assuming that it is initialized from a non-turbulent situation, the turbulence must have development along a roughly 1000 m long path with a steep slope of 17–21° (Fig. 1). The combination of a steep slope and non-uniform terrain along the slope are favorable conditions for a fast development of mechanically induced turbulence. Strong shear stress values (τ) during jet periods (Fig. 8), as caused by friction between the canopy and the air moving downslope support this interpretation.

Since the mountain ridge is located upwind of the measurement site, it is highly likely that the jet periods are caused by local processes such as surface cooling (e.g. katabatic flows such as ACDF), topographic effects such as mountain waves that initiate katabatic flows (Banta et al., 2004), and a terrain that is either favorable or adverse for building up pressure gradients. Larger-scale synoptic forcing such as the propagation of a front as described by Sheridan and Vosper (2012), is not likely to have occurred because synoptic-scale pressure gradients are rather small and the frontal approach as generally applied in the high latitudes, does not apply in the tropics and subtropics (Riehl, 1954).

4.2 Jet periods and turbulent exchange

The nocturnal turbulent exchange depends mostly on atmospheric conditions such as wind speed and atmospheric stability. During strongly stable conditions the turbulence

BGD
11, 4695–4727, 2014

is very weak and not well developed, and therefore the fluxes are small and the CO_2 accumulates near the surface. This is apparent from CO_2-profiles (Fig. 5), vertical wind velocities (Figs. 2 and 7), and fluxes of sensible heat, latent heat, CO_2, and the friction velocity (Fig. 8) for periods before and after jet periods. For cases with constant and strong turbulence (e.g. due to strong winds), an accumulation of CO_2 is inhibited due to a constant mixing of air above and below the canopy. Under these conditions, turbulent fluxes are more or less constant and small (Oliveira et al., 2013). Before a jet period occurs, strongly stable conditions prevail during which accumulation of CO_2 takes place (Fig. 5, 22:30–23:00 LT). Discontinuities in the time- and frequency-domains of the spectrogram (Fig. 7) indicate that stable boundary layer conditions inhibit the development of turbulence. Even if turbulence occurs e.g. due to friction, it is immediately suppressed. After the subsequent onset of a jet period (Figs. 2, 5 and 7, 23:30–00:30 LT) the intense mixing of air can cause strong CO_2 fluxes into the atmosphere (Fig. 9, 23:30–00:30 LT). Once the stored CO_2 is released and the vertical gradient is reduced, the magnitude of the flux will be reduced, too.

As compared to no-jet periods, the sensible heat fluxes during jet periods are frequently more negative and of larger magnitude (Figs. 8 and 9). Strong surface cooling during the night leads to temperature inversions. As shown in Wolfelmaier et al. (1999), LLJ and katabatic flows are likely to occur at the top of temperature inversions in complex terrain. The resulting turbulence mixes warm air from above and cold air from the canopy surface. This leads to exclusively negative and strong sensible heat fluxes (Figs. 8 and 9). The results also indicate a temporal increase in air temperature (data not shown). These results match the findings of Pinto et al. (2006) from T-REX.

4.3 Duration and ending of jet periods

The longest jet period observed in this study lasted for 110 min and was a LLJ. These are rather short time periods in comparison to those observed at other sites, especially flat terrain sites, where a LLJ can last throughout the night until the beginning of dawn (e.g. Whiteman et al., 1997; Banta et al., 2007; Duarte et al., 2012). On the other

BGD
11, 4695–4727, 2014

hand, the shortest duration of a jet period (30 min) is too long to be explained only by the occurrence of gusts (Acevedo et al., 2006) and the vertical wind profiles provide no indication of gusts during jet periods. Results of Pinto et al. (2006) and Chiao and Dumais (2013) from the VTMX and T-REX project, respectively, show longer duration and larger depth of the detected jets on a larger topographic scale. The CLM valley is roughly 2 km wide and 8 km long (Fig. 1) while the Great Salt Lake Valley and Owens Valley (where VTMX and T-REX were performed) are much larger (about 5 to 10 times). This indicates that jets can occur on various spatial scales and that their duration is depending on the size of the valley.

Mahrt et al. (2010) describe that drainage flows are likely to disappear at a certain height once the cold air pool has grown to that specific height. The experimental towers at CLM are located at the upper part of the valley (Fig. 1). Due to the structure of the valley and the unrestricted outflow of cold air, it is very unlikely that the cold pool ever reaches the towers (Fig. 1). Therefore, such conditions are very unlikely to be the cause for the termination of the jet periods.

A process that is retrieved from large eddy simulation results and which is described by Zhou and Chow (2012, 2013), offers an explanation for the observed uphill flows at the end of the jet periods: surface cooling leads to a katabatic flow (Fig. 10, top panel). It flows down the valley until it reaches the height of neutral buoyancy. If the momentum of the katabatic flow is high, it overshoots the height of neutral buoyancy and dives into air masses of lower temperatures and higher density. At this point, it experiences positive buoyancy and flows upwards until it reaches the point of neutral buoyancy again. Such counter flows may either maintain their horizontal wind direction and only change the direction of the vertical wind component (Fig. 10, middle panel) or they change horizontal wind direction and the direction of the vertical wind component, which results in an up-slope-flow (Fig. 10, bottom panel).

At the Chi-Lan Mountain site, both LLJ and ACDF follow the terrain downhill, therefore it is possible for both to overshoot the point of neutral buoyancy in the described way. Depending on the stratification of the boundary layer and the strength of the jet

BGD
11, 4695–4727, 2014

period, both a vertical air motion (Figs. 2 and 4) and an uphill flow (Fig. 3) may establish the state of equilibrium.

5 Conclusions

With the use of a SODAR with high vertical resolution (5 m) and a vertical range of 300 m it was possible to identify two types of nocturnal flows that cause intermittent turbulence in very complex terrain. With the help of two eddy-covariance set-ups, employed as an extension of the vertical wind profile of the SODAR, a clear distinction between LLJ and ACDF was possible. Effects of LLJ and ACDF on turbulent exchange processes and data quality could be quantified and shown to be very similar for both cases.

The causes and driving processes for LLJ and ADCF periods could not be completely clarified but a stable stratification and the terrain of the valley play a major role. However, gusts or large scale wind systems could be excluded as a source.

Profile measurements of CO_2 clearly showed that strong CO_2 fluxes during the jet periods were caused by a decay of a CO_2 pool that had accumulated during calm conditions before the jet period. Nocturnal LLJ and ACDF can lead to a coupling of above-canopy and below-canopy air and therefore result in strong fluxes of mass and energy. Due to their frequent occurrence jet periods play a major role for the nocturnal turbulent exchange at CLM.

It is evident from the presented data that jet periods lead to canopy exchange processes that are considerably different from those during their absence. Although eddy-covariance data quality during no-jet periods is lower than during jet periods, which makes a comparison of the fluxes difficult, it is evident that fluxes are generally smaller in the absence of LLJ and ACDF. For sites with frequent occurrence of intermittent turbulence this should be taken into account. Therefore, long-term datasets should be analyzed carefully to avoid any overestimate of nocturnal fluxes due to gap-filling algorithms or to flagging high flux data during quality control.

BGD
11, 4695–4727, 2014

This work provided measurements of upslope moving air in nocturnal stable boundary layer conditions. This phenomenon occurred for only about 10 to 20 min at the end of LLJ and ACDF events. It appears to be caused by an overshooting of LLJ or ACDF below the point of neutral buoyancy and the respective equalization during which air can flow upslope.

Acknowledgements. This work was supported by the Deutsche Forschungsgemeinschaft (DFG) through project KL623/10-1. The authors thank Niels Thiermann from Scintec, Shih-Chieh Chang, Shih-Bin Ding, Natchaya Pingintha, and Pei-Ling for the great support of our field work at CLM.

References

Acevedo, O. C., Moraes, O. L. L., Degrazia, G. A., and Medeiros, L. E.: Intermittency and the exchange of scalars in the nocturnal surface layer, Bound.-Lay. Meteorol., 119, 41–55, doi:10.1007/s10546-005-9019-3, 2006.

Aubinet, M.: Eddy covariance CO_2 flux measurements in nocturnal conditions: an analysis of the problem, Ecol. Appl., 18, 1368–1378, 2008.

Aubinet, M., Berbigier, P., Bernhofer, C. H., Cescatti, A., Feigenwinter, C., Granier, A., Grunwald, T. H., Havrankova, K., Heinesch, B., Longdoz, B., Marcolla, B., Montagnani, L., and Sedlak, P.: Comparing CO_2 storage and advection conditions at night at different carboeuroflux sites, Bound.-Lay. Meteorol., 116, 63–94, doi:10.1007/s10546-004-7091-8, 2005.

Banta, R. M., Newsom, R. K., Lundquist, J. K., Pichugina, Y. L., Coulter, R. L., and Mahrt, L.: Nocturnal low-level jet characteristics over kansas during cases-99, Bound.-Lay. Meteorol., 105, 221–252, doi:10.1023/A:1019992330866, 2002.

Banta, R. M., Darby, L. S., Fast, J. D., Pinto, J. O., Whiteman, C. D., Shaw, W. J., and Orr, B. W.: Nocturnal low-level jet in a mountain basin complex, Part 1: Evolution and effects on local flows, J. Appl. Meteorol., 43, 1348–1365, 2004.

Banta, R. M., Mahrt, L., Vickers, D., Sun, J., Balsley, B. B., Pichugina, Y. L., and Williams, E. L.: The very stable boundary layer on nights with weak low-level jets, J. Atmos. Sci., 64, 3068–3090, doi:10.1175/Jas4002.1, 2007.

BGD
11, 4695–4727, 2014

Belcher, S. E., Finnigan, J. J., and Harman, I. N.: Flows through forest canopies in complex terrain, Ecol. Appl., 18, 1436–1453, 2008.
Chang, S. C., Lai, I. L., and Wu, J. T.: Estimation of fog deposition on epiphytic bryophytes in a subtropical montane forest ecosystem in northeastern taiwan, Atmos. Res., 64, 159–167, 2002.
Chiao, S. and Dumais, R.: A down-valley low-level jet event during T-REX 2006, Meteorol. Atmos. Phys., 122, 75–90, doi:10.1007/s00703-013-0279-z, 2013.
Choukulkar, A., Calhoun, R., Billings, B., and Doyle, J.: Investigation of a complex nocturnal flow in owens valley, california using coherent doppler lidar, Bound.-Lay. Meteorol., 144, 359–378, doi:10.1007/s10546-012-9729-2, 2012.
Cooper, D. I., Leclerc, M. Y., Archuleta, J., Coulter, R., Eichinger, W. E., Kao, C. Y. J., and Nappo, C. J.: Mass exchange in the stable boundary layer by coherent structures, Agr. Forest Meteorol., 136, 114–131, doi:10.1016/j.agrformet.2004.12.012, 2006.
Darby, L. S., Allwine, K. J., and Banta, R. M.: Nocturnal low-level jet in a mountain basin complex, Part 2: Transport and diffusion of tracer under stable conditions, J. Appl. Meteorol. Clim., 45, 740–753, doi:10.1175/Jam2367.1, 2006.
Doran, J. C., Fast, J. D., and Horel, J.: The VTMX 2000 campaign, B. Am. Meteorol. Soc., 83, 537–551, doi:10.1175/1520-0477(2002)083<0537:Tvc>2.3.Co;2, 2002.
Duarte, H. F., Leclerc, M. Y., and Zhang, G. S.: Assessing the shear-sheltering theory applied to low-level jets in the nocturnal stable boundary layer, Theor. Appl. Climatol., 110, 359–371, doi:10.1007/s00704-012-0621-2, 2012.
Durden, D. J., Nappo, C. J., Leclerc, M. Y., Duarte, H. F., Zhang, G., Parker, M. J., and Kurzeja, R. J.: On the impact of wave-like disturbances on turbulent fluxes and turbulence statistics in nighttime conditions: a case study, Biogeosciences, 10, 8433–8443, doi:10.5194/bg-10-8433-2013, 2013.
El-Madany, T. S., Griessbaum, F., Fratini, G., Juang, J. Y., Chang, S. C., and Klemm, O.: Comparison of sonic anemometer performance under foggy conditions, Agr. Forest Meteorol., 173, 63–73, doi:10.1016/j.agrformet.2013.01.005, 2013.
Foken, T.: Micrometeorology, Springer, Berlin and Heidelberg, 328 pp., 2008.
Foken, T. and Wichura, B.: Tools for quality assessment of surface-based flux measurements, Agr. Forest Meteorol., 78, 83–105, 1996.

BGD
11, 4695–4727, 2014

Goulden, M. L., Munger, J. W., Fan, S. M., Daube, B. C., and Wofsy, S. C.: Measurements of carbon sequestration by long-term eddy covariance: methods and a critical evaluation of accuracy, Glob. Change Biol., 2, 169–182, 1996.

Grubisic, V., Doyle, J. D., Kuettner, J., Mobbs, S., Smith, R. B., Whiteman, C. D., Dirks, R., Czyzyk, S., Cohn, S. A., Vosper, S., Weissmann, M., Haimov, S., De Wekker, S. F. J., Pan, L. L., and Chow, F. K.: The terrain-induced rotor experiment a field campaign overview including observational highlights, B. Am. Meteorol. Soc., 89, 1513–1533, doi:10.1175/2008bams2487.1, 2008.

Huang, J. and Bou-Zeid, E.: Turbulence and vertical fluxes in the stable atmospheric boundary layer, Part 1: A large-eddy simulation study, J. Atmos. Sci., 70, 1513–1527, doi:10.1175/Jas-D-12-0167.1, 2013.

Karipot, A., Leclerc, M. Y., Zhang, G. S., Lewin, K. F., Nagy, J., Hendrey, G. R., and Starr, G.: Influence of nocturnal low-level jet on turbulence structure and CO_2 flux measurements over a forest canopy, J. Geophys. Res.-Atmos., 113, D10102, doi:10.1029/2007jd009149, 2008.

Klemm, O., Chang, S. C., and Hsia, Y.: Energy fluxes at a subtropical mountain cloud forest, Forest Ecol. Manag., 224, 5–10, doi:10.1016/j.foreco.2005.12.003, 2006.

Kutsch, W. L., Kolle, O., Rebmann, C., Knohl, A., Ziegler, W., and Schulze, E. D.: Advection and resulting CO_2 exchange uncertainty in a tall forest in central germany, Ecol. Appl., 18, 1391–1405, 2008.

Lee, X. H.: A model for scalar advection inside canopies and application to footprint investigation, Agr. Forest Meteorol., 127, 131–141, doi:10.1016/j.agrformet.2004.07.009, 2004.

Lee, X., Neumann, H. H., DenHartog, G., Fuentes, J. D., Black, T. A., Mickle, R. E., Yang, P. C., and Blanken, P. D.: Observation of gravity waves in a boreal forest, Bound.-Lay. Meteorol., 84, 383–398, doi:10.1023/A:1000454030493, 1997.

Lee, X., Massman, W., and Law, B.: Handbook of Micrometeorology – a Guide for Surface Flux Measurement and Analysis, Kluwer Academic Press, Dordrecht, 250 pp., 2004.

Mahrt, L.: Stratified atmospheric boundary layers, Bound.-Lay. Meteorol., 90, 375–396, doi:10.1023/A:1001765727956, 1999.

Mahrt, L.: Computing turbulent fluxes near the surface: needed improvements, Agr. Forest Meteorol., 150, 501–509, doi:10.1016/j.agrformet.2010.01.015, 2010.

Mahrt, L., Richardson, S., Seaman, N., and Stauffer, D.: Non-stationary drainage flows and motions in the cold pool, Tellus A, 62, 698–705, doi:10.1111/j.1600-0870.2010.00473.x, 2010.

BGD
11, 4695–4727, 2014

Mathieu, N., Strachan, I. B., Leclerc, M. Y., Karipot, A., and Pattey, E.: Role of low-level jets and boundary-layer properties on the nbl budget technique, Agr. Forest Meteorol., 135, 35–43, doi:10.1016/j.agrformet.2005.10.001, 2005.

Mauder, M. and Foken, T.: Documentation and instruction manual of the eddy-covariance software package tk3, Universität Bayreuth, Abteilung Mikrometeorologie, Arbeitsergebnisse, 46, 2011.

Mauder, M., Cuntz, M., Drüe, C., Graf, A., Rebmann, C., Schmid, H. P., Schmidt, M., and Steinbrecher, R.: A strategy for quality and uncertainty assessment of long-term eddy-covariance measurements, Agr. Forest Meteorol., 169, 122–135, doi:10.1016/j.agrformet.2012.09.006, 2013.

Moncrieff, J. B., Massheder, J. M., deBruin, H., Elbers, J., Friborg, T., Heusinkveld, B., Kabat, P., Scott, S., Soegaard, H., and Verhoef, A.: A system to measure surface fluxes of momentum, sensible heat, water vapour and carbon dioxide, J. Hydrol., 189, 589–611, 1997.

Nakamura, R. and Mahrt, L.: A study of intermittent turbulence with cases-99 tower measurements, Bound.-Lay. Meteorol., 114, 367–387, 2005.

Oliveira, P. E. S., Acevedo, O. C., Moraes, O. L. L., Zimermann, H. R., and Teichrieb, C.: Nocturnal intermittent coupling between the interior of a pine forest and the air above it, Bound.-Lay. Meteorol., 146, 45–64, doi:10.1007/s10546-012-9756-z, 2013.

Pinto, J. O., Parsons, D. B., Brown, W. O. J., Cohn, S., Chamberlain, N., and Morley, B.: Coevolution of down-valley flow and the nocturnal boundary layer in complex terrain, J. Appl. Meteorol. Clim., 45, 1429–1449, 2006.

Reinecke, P. A. and Durran, D. R.: Initial-condition sensitivities and the predictability of downslope winds, J. Atmos. Sci., 66, 3401–3418, doi:10.1175/2009jas3023.1, 2009.

Riehl, H.: Tropical Meteorology, McGraw-Hill, New York, 392 pp., 1954.

Sheridan, P. and Vosper, S.: High-resolution simulations of lee waves and downslope winds over the Sierra Nevada during T-REX IOP 6, J. Appl. Meteorol. Clim., 51, 1333–1352, doi:10.1175/Jamc-D-11-0207.1, 2012.

Stull, R. B.: An Introduction to Boundary Layer Meteorology, Kluwer Academic Publishers, Dordrecht, Boston, London, 666 pp., 1988.

Sun, J. L., Mahrt, L., Banta, R. M., and Pichugina, Y. L.: Turbulence regimes and turbulence intermittency in the stable boundary layer during cases-99, J. Atmos. Sci., 69, 338–351, doi:10.1175/Jas-D-11-082.1, 2012.

BGD
11, 4695–4727, 2014

Vecenaj, Z., De Wekker, S. F. J., and Grubisic, V.: Near-surface characteristics of the turbulence structure during a mountain-wave event, J. Appl. Meteorol. Clim., 50, 1088–1106, doi:10.1175/2010jamc2450.1, 2011.
Webb, E. K., Pearman, G. I., and Leuning, R.: Correction of flux measurements for density effects due to heat and water-vapor transfer, Q. J. Roy. Meteor. Soc., 106, 85–100, 1980.
Whiteman, C. D., Bian, X. D., and Zhong, S. Y.: Low-level jet climatology from enhanced rawinsonde observations at a site in the southern great plains, J. Appl. Meteorol., 36, 1363–1376, doi:10.1175/1520-0450(1997)036<1363:Lljcfe>2.0.Co;2, 1997.
Wilczak, J. M., Oncley, S. P., and Stage, S. A.: Sonic anemometer tilt correction algorithms, Bound.-Lay. Meteorol., 99, 127–150, 2001.
Wolfelmaier, F. A., King, C. W., Mursch-Radlgruber, E., and Rengarajan, G.: Mini-sodar observations of drainage flows in the rocky mountains, Theor. Appl. Climatol., 64, 83–91, 1999.
Zangl, G.: The impact of weak synoptic forcing on the valley-wind circulation in the alpine inn valley, Meteorol. Atmos. Phys., 105, 37–53, doi:10.1007/s00703-009-0030-y, 2009.
Zeri, M. and Sa, L. D. A.: Horizontal and vertical turbulent fluxes forced by a gravity wave event in the nocturnal atmospheric surface layer over the amazon forest, Bound.-Lay. Meteorol., 138, 413–431, doi:10.1007/s10546-010-9563-3, 2011.
Zhou, B. and Chow, F. K.: Nighttime cold-air intrusions and transient warming in a steep valley: a nested large-eddy simulation study, 15th Conference on Mountain Meteorology, Steamboat Springs, Abstract no. 3.2, Colorado, 19–24 August 2012, 2012.
Zhou, B. W. and Chow, F. K.: Nested large-eddy simulations of the intermittently turbulent stable atmospheric boundary layer over real terrain, J. Atmos. Sci., 70, 3262–3276, doi:10.1175/Jas-D-13-02.1, 2013.
Zilitinkevich, S. S., Elperin, T., Kleeorin, N., L'vov, V., and Rogachevskii, I.: Energy- and flux-budget turbulence closure model for stably stratified flows, Part 2: The role of internal gravity waves, Bound.-Lay. Meteorol., 133, 139–164, doi:10.1007/s10546-009-9424-0, 2009.

BGD
11, 4695–4727, 2014

Table 1. Fourteen jet periods during the experimental period with their duration, maximum wind speed, height of maximum wind speed, and the resulting classification as LLJ or ACDF.

Date	Duration (hh:mm LT)	Max. wind speed ($m s^{-1}$)	Height of max wind speed (m)	Classification
27 Jun	00:30–01:00	3	Canopy	ACDF
28 Jun	02:00–02:40	5	100	LLJ
29 Jun	04:40–05:40	6	130	LLJ
29–30 Jun	23:20–01:00	7	Canopy	ACDF
1 Jul	00:40–01:10	3	100	LLJ
1 Jul	02:40–03:10	2	Canopy	ACDF
3 Jul	20:30–22:20	11	180	LLJ
4 Jul	20:20–21:40	14	240	LLJ
7 Jul	04:00–04:30	4	Canopy	ACDF
7 Jul	21:50–23:20	4	Canopy	ACDF
8–9 Jul	23:10–00:30	7	100	LLJ
9 Jul	22:50–23:50	5	80	LLJ
11 Jul	00:20–02:10	6	90	LLJ
14 Jul	01:50–02:30	3	Canopy	ACDF

BGD
11, 4695–4727, 2014

Table 2. Percentiles of stability parameter (ζ), wind speed ($m\,s^{-1}$), and TKE (turbulent kinetic energy in $m^2\,s^{-2}$) at height 5 m and 10 m above canopy for jet and no-jet periods.

Parameter	height	ζ			wind speed			TKE		
Percentile		25th	50th	75th	25th	50th	75th	25th	50th	75th
no-jet period	5	0.092	0.212	0.356	1.09	1.54	1.95	0.174	0.232	0.349
jet period	5	0.112	0.208	0.381	1.29	2.18	2.89	0.218	0.358	0.706
no-jet period	10	0.026	0.341	0.874	1.33	1.91	2.27	0.140	0.191	0.270
jet period	10	0.278	0.615	0.942	1.63	2.23	2.83	0.187	0.311	0.624

BGD
11, 4695–4727, 2014

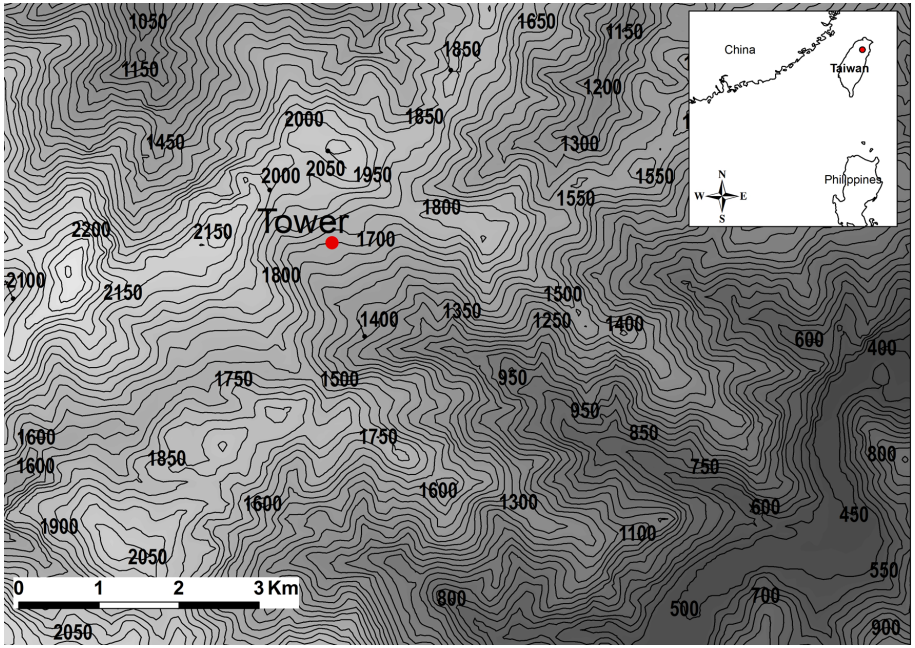

Fig. 1. Topographic map of the studied valley and the surrounding topography. Numbers indicate the height a.s.l. (m) for the respective contour lines. The Tower with the eddy-covariance and profile measurements is indicated by a red dot. Light colors denote high elevation and dark colors low elevations.

BGD
11, 4695–4727, 2014

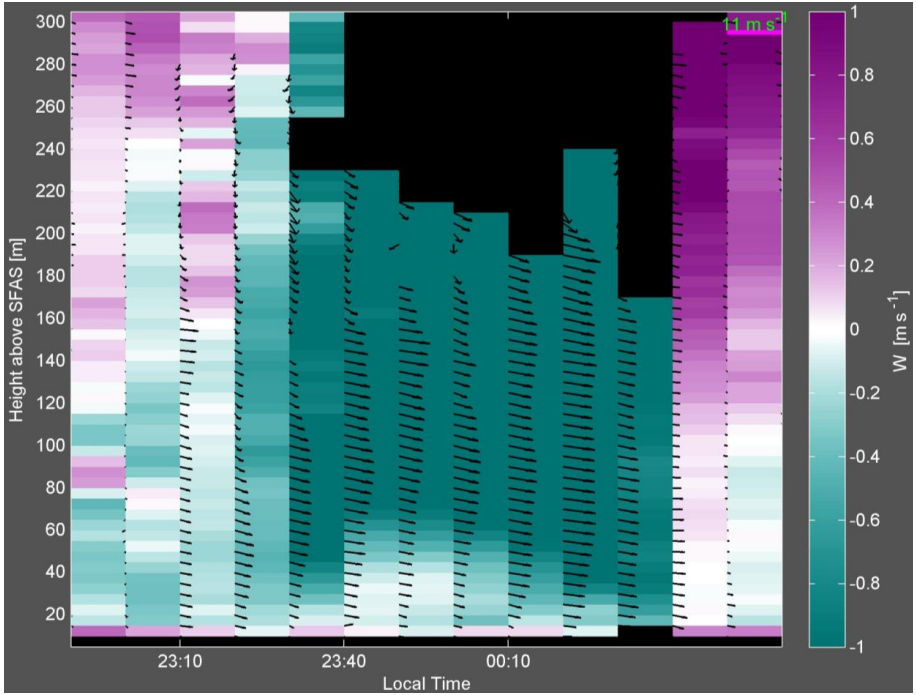

Fig. 2. Low-level jet event from 8 July 22:50–9 July 01:00. Black arrows are wind vectors indicating wind speed (length) and wind direction (orientation). The width of one 10 min column corresponds to a wind speed of 11 m s^{-1}. The vertical wind speed is shown by the background colors. Positive vertical wind speeds are directed upwards and negative wind speeds are directed downwards. Positive vertical wind speeds are denoted with white to purple colors while negative vertical wind speeds are white to teal. Wind speeds around zero are white. The timestamps and the beginning of the black arrows are located at the left side of the corresponding columns.

BGD
11, 4695–4727, 2014

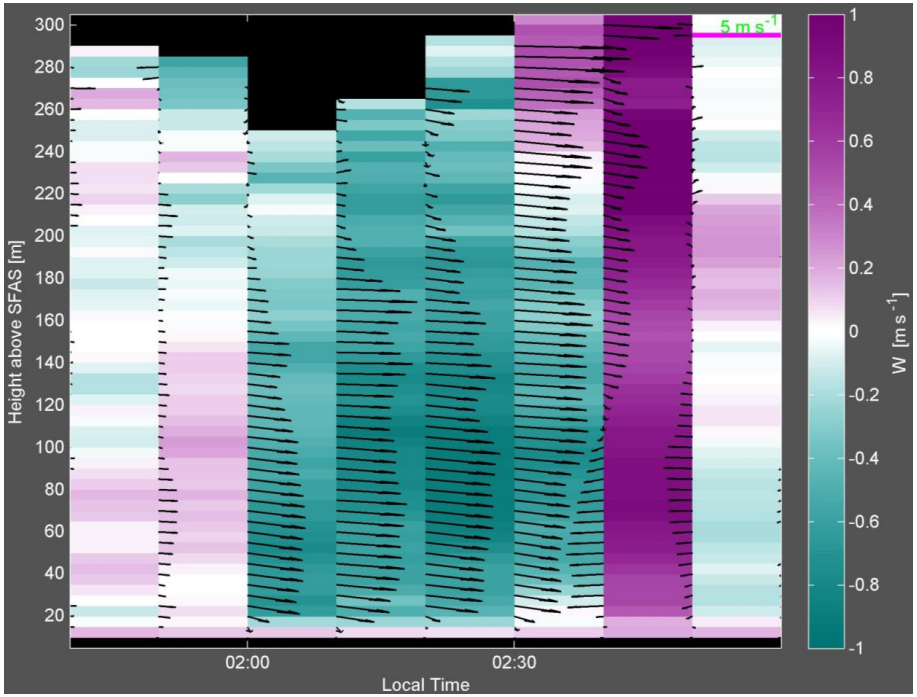

Fig. 3. Same as Fig. 2 but from 28 June 01:40–02:50. The width of one 10 min column corresponds to a wind speed of 5 m s^{-1}.

BGD
11, 4695–4727, 2014

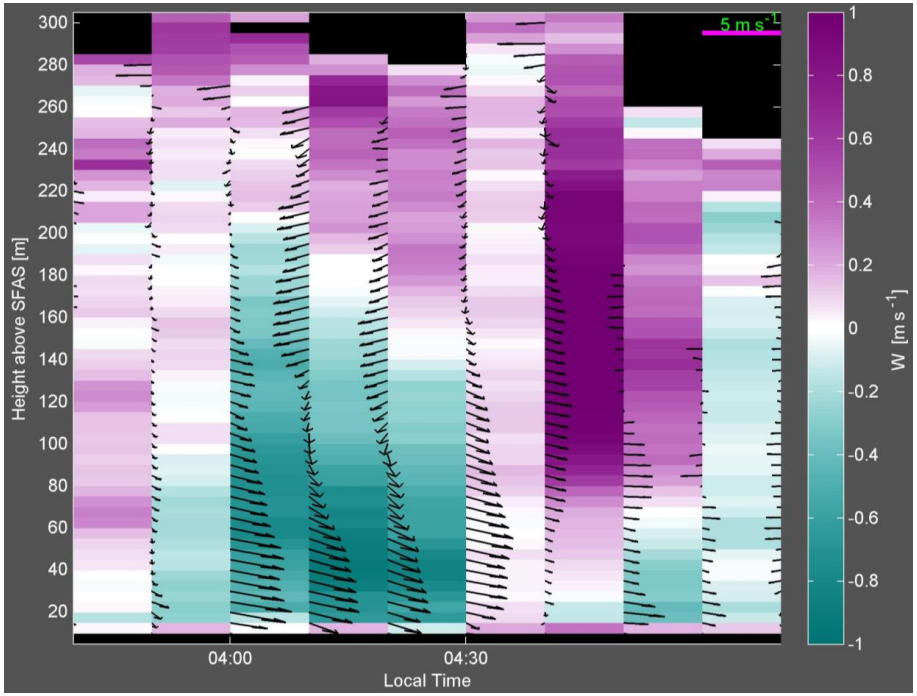

Fig. 4. Same as Fig. 3 but for an ACDF from 7 July 03:40–05:10.

BGD
11, 4695–4727, 2014

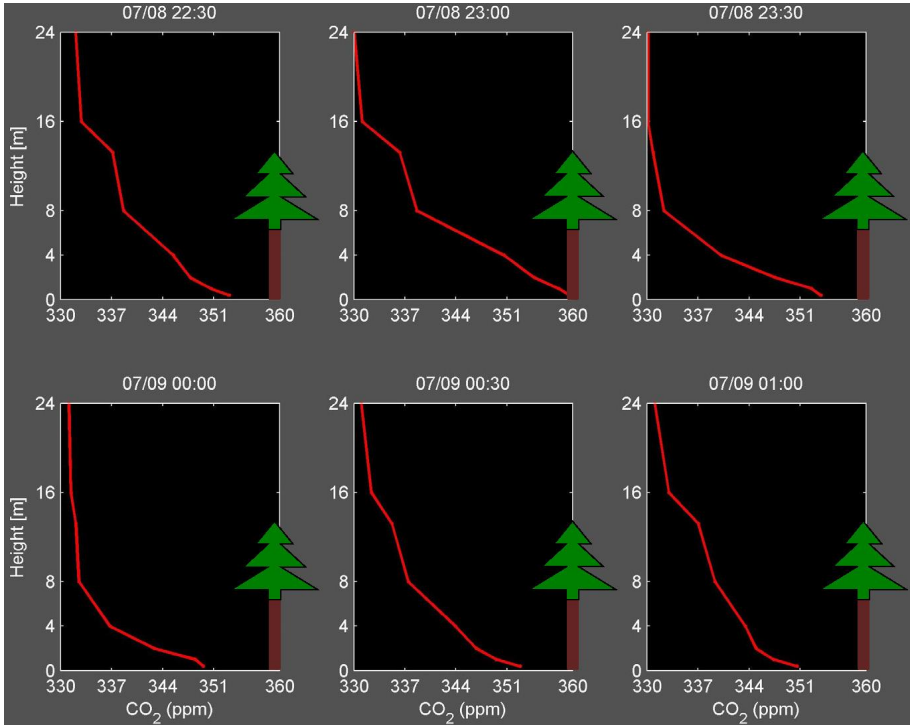

Fig. 5. 30 min averaged CO_2-profiles from 8 measurement heights from 8 July, 22:30 LT to 9 July, 01:00 LT. The tree scheme indicates the location of the canopy and the trunk space with respect to the profile measurement points. The 23:30 and the 00:00 profiles are during the LLJ of Fig. 2. The time stamps indicate the beginning of the 30 min averaging period for the respective profiles.

BGD
11, 4695–4727, 2014

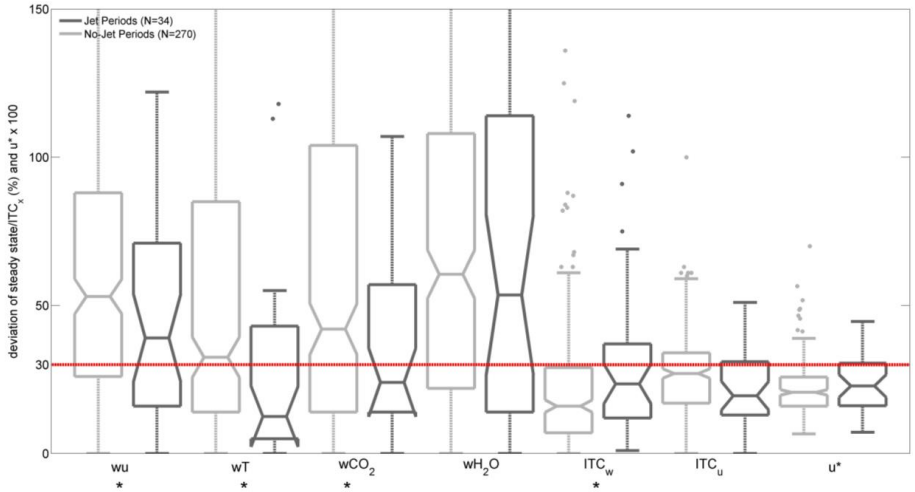

Fig. 6. Box plots of percentile deviation of steady state for time series of vertical wind velocity with streamwise wind velocity, temperature, CO_2 and H_2O (wu, wT, wCO_2, wH_2O) as well as percentile deviations of measured integral turbulence characteristics from modeled values for vertical and streamwise wind velocity (ITC_w, ITC_u), and the friction velocity (u^*), multiplied by 100 to fit the scale. Box plots for no-jet periods are plotted in light grey while jet periods are plotted in dark grey. Stars denote significant differences between jet- and no-jet periods. The red line at the value of 30 represents the thresholds for the best quality class. It represents a 30 % deviation of the ITC- and steady state criteria as well as a friction velocity of 0.3 m s^{-1}. The Whiskers are set to 1.5 interquartile range and the boxes are waisted to accentuate the median value.

BGD
11, 4695–4727, 2014

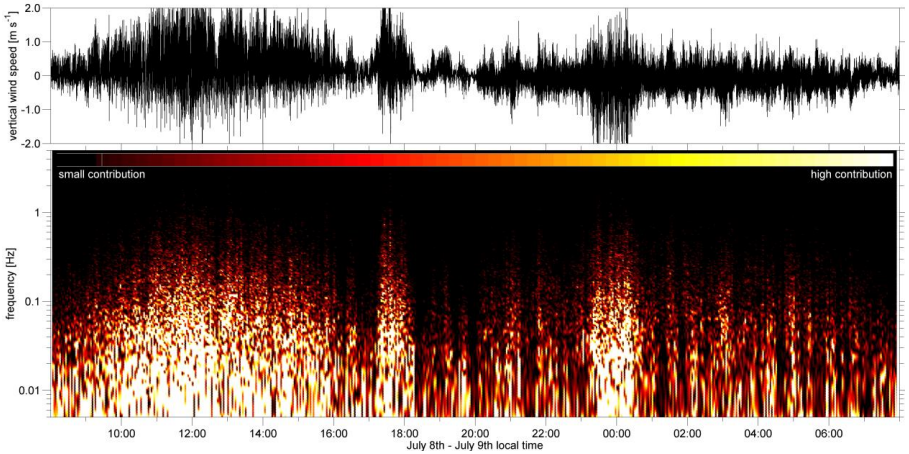

Fig. 7. Top panel: twenty-four hour time series of 10 Hz vertical wind velocity data as measured with the sonic anemometer at 10 m above canopy. Bottom panel: spectrogram of the vertical wind velocity data from the top panel. Dark colors indicate frequencies with small contributions to power spectral density ($m s^{-2}$) while light colors indicate high contributions from the respective frequencies.

BGD
11, 4695–4727, 2014

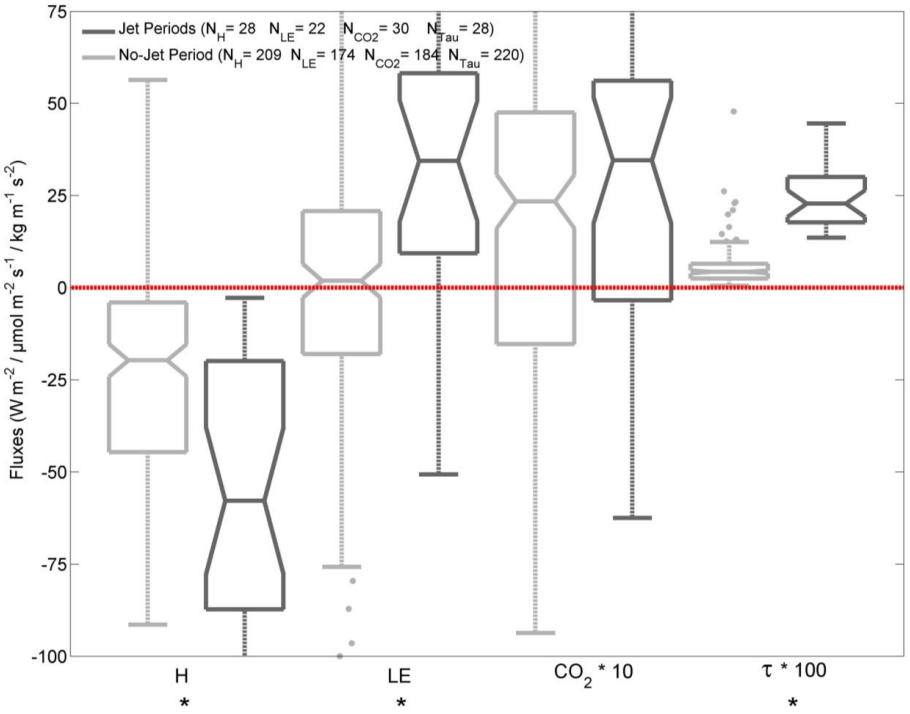

Fig. 8. Box plots of sensible heat flux H ($W m^{-2}$), latent heat flux LE ($W m^{-2}$), CO_2 flux ($\mu mol\, m^{-2}\, s^{-1}$), and shear stress τ ($kg\, m^{-1}\, s^{-2}$) for the jet periods (dark grey) and the no-jet periods (light grey). CO_2 flux values were multiplied by 10 and shear stress values by 100 to fit the scale. Stars denote significant differences between no-jet and jet periods. N_x gives the number of 30 min files used in the analysis. The Whiskers are set to 1.5 interquartile range and the boxes are waisted to accentuate the median value.

BGD
11, 4695–4727, 2014

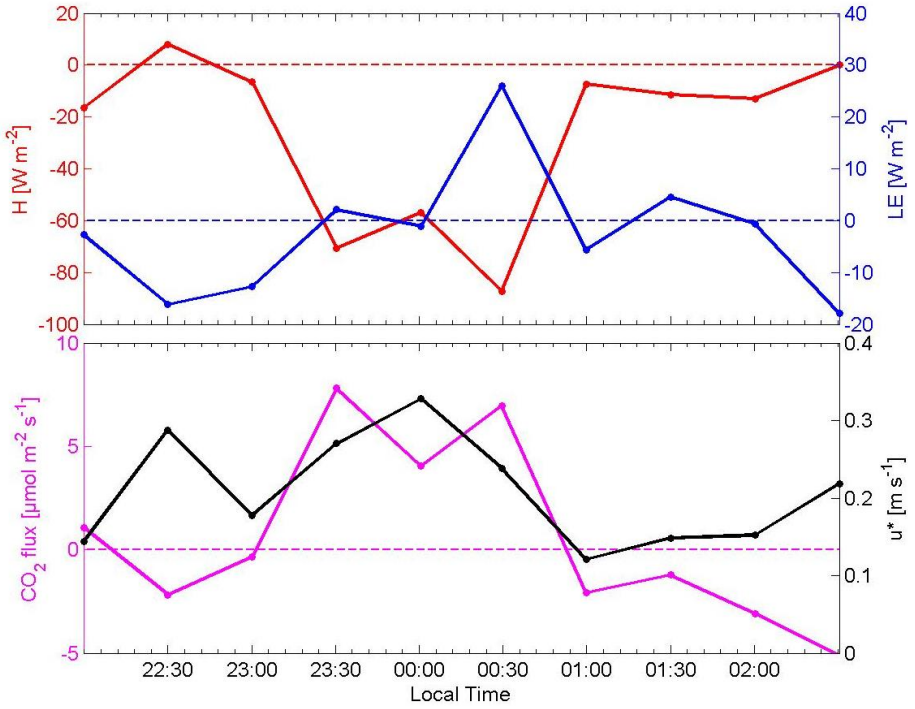

Fig. 9. Fluxes of sensible heat (H, red), latent heat (LE, blue), CO_2 (magenta) and friction velocity (u^*, black) for the LLJ from 8 July 23:30–9 July 00:30 (Fig. 2). Dashed lines indicate zero lines of the respective variables.

BGD
11, 4695–4727, 2014

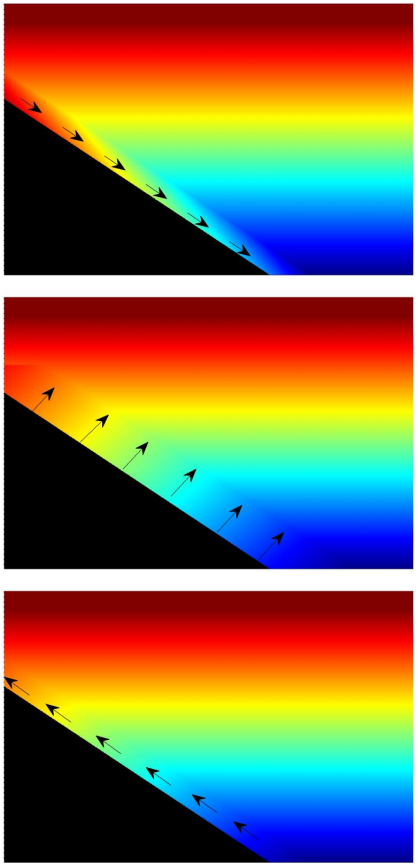

Fig. 10. Scheme of the above canopy drainage (top) and the respective counter flows (middle and bottom) at the end of the ACDF. Color scale indicates temperatures ranging from cooler temperatures (blue) to warmer temperatures (red). Arrows show the wind direction. Black surface represents the slope of the valley.

BGD
11, 4695–4727, 2014